



Does acetone react with HO₂ in the upper-troposphere?

T. J. Dillon¹, A. Pozzer^{1,2,3}, L. Vereecken¹, J. N. Crowley¹, and J. Lelieveld^{1,2,4}

¹Max-Planck-Institute für Chemie, Atmospheric Chemistry Division, Mainz, Germany

²EEWRC, Cyprus Institute, Nicosia, Cyprus

³ICTP, Earth System Physics, Trieste, Italy

⁴King Saud University, Riyadh, Saudi Arabia

Correspondence to: T. J. Dillon (terry.dillon@mpic.de)

Received: 14 June 2010 – Published in Atmos. Chem. Phys. Discuss.: 5 July 2010

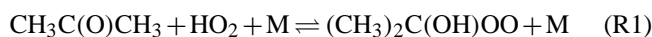
Revised: 18 January 2012 – Accepted: 19 January 2012 – Published: 2 February 2012

Abstract. Recent theoretical calculations showed that reaction with HO₂ could be an important sink for acetone (CH₃C(O)CH₃) and source of acetic acid (CH₃C(O)OH) in cold parts of the atmosphere (e.g. the tropopause region). This work details studies of HO₂ + CH₃C(O)CH₃ (CH₃)₂C(OH)OO (R1) in laboratory-based and theoretical chemistry experiments; the atmospheric significance of Reaction (R1) was assessed in a global 3-D chemical model. Pulsed laser-kinetic experiments were conducted, for the first time, at the low-temperatures representative of the tropopause. Reaction with NO converted HO₂ to OH for detection by laser induced fluorescence. Reduced yields of OH at $T < 220$ K provided indirect evidence for the sequestration of HO₂ by CH₃C(O)CH₃ with a forward rate coefficient greater than 2×10^{-12} cm³ molecule⁻¹ s⁻¹. No evidence for Reaction (R1) was observed at $T > 230$ K, probably due to rapid thermal dissociation back to HO₂ + CH₃C(O)CH₃. Numerical simulations of the data indicate that these experiments were sensitive to only (R1a) HO₂-CH₃C(O)CH₃ complex formation, the first step in (R1). Rearrangement (R1b) of the complex to form peroxy radicals, and hence the atmospheric significance of (R1) has yet to be rigorously verified by experiment.

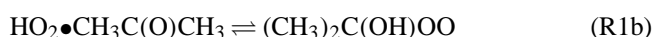
Results from new quantum chemical calculations indicate that K_1 is characterised by large uncertainties of at least an order of magnitude at $T < 220$ K. The large predicted values from Hermans et al. lie at the top end of the range of values obtained from calculations at different (higher) levels of theory. Atmospheric modelling studies demonstrated that whilst (R1) chemistry may be a significant loss process for CH₃C(O)CH₃ near the tropopause, it cannot explain observations of CH₃C(O)OH throughout the troposphere.

1 Introduction

Acetone, CH₃C(O)CH₃, is emitted by vegetation, biomass burning, the oceans and industry at ~ 95 Tg yr⁻¹ (Jacob et al., 2002). The long lifetime of CH₃C(O)CH₃ near the surface allows for transport out of the boundary layer (Atkinson and Arey, 2003). In the cold, dry upper troposphere (UT), CH₃C(O)CH₃ photolysis may be an important initiator of free-radical chemistry, leading to generation of O₃ and OH, the primary oxidant in the troposphere (Arnold et al., 1986; Singh et al., 1995; McKeen et al., 1997; Wennberg et al., 1998; Arnold et al., 2005). It was recently proposed (Hermans et al., 2004) that reaction with HO₂ (R1) initiates degradation of CH₃C(O)CH₃ in the UT.



Using quantum-chemical and statistical rate calculations, Hermans et al. (2004) studied the (R1) equilibrium (in reality an association and rearrangement), and derived an overall $K_1(T) = 7.8 \times 10^{-28} \exp(7180/T)$. The finer mechanistic details of the two-step (R1) process are unimportant when assessing atmospheric impact, but can lead to complications in interpretation of laboratory data. The first HO₂-CH₃C(O)CH₃ complex formation step (here denoted R1a), was identified in the theoretical calculations of first Aloisio and Francisco (2000) and then Hermans et al. (2005); experimental evidence for the (R1a) equilibrium has recently been published by Grieman et al. (2011)



The complex is a 7-membered ring structure whereby HO₂ is bound between the carbonyl group and an H from a methyl

group of CH₃C(O)CH₃. Concerted addition of the terminal O of HO₂ to the carbonyl C, and H-atom transfer from HO₂ to the carbonyl O (R1b) completes (R1). Hermans et al. (2004) report that at $T < 220$ K, (R1) proceeds rapidly ($k_1 > 1 \times 10^{-12}$ cm³ molecule⁻¹ s⁻¹) with formation of significant quantities of (CH₃)₂C(OH)OO as the reverse reaction is slow ($k_{-1} < 20$ s⁻¹). CH₃C(O)CH₃ degradation is completed by subsequent reactions of (CH₃)₂C(OH)OO. In the UT this is mainly with NO (R2) and to a lesser extent HO₂ and other radicals.



The key features of (R1–R2) chemistry of interest in the atmosphere or in this work are depicted on Fig. 1.

Using typical tropopause conditions of $T = 200$ K, $[\text{OH}] = 6 \times 10^5$, $[\text{HO}_2] = 2.5 \times 10^7$ and $[\text{NO}] = 4 \times 10^8$ molecule cm⁻³, Hermans et al. (2004) calculated an effective CH₃C(O)CH₃ removal rate via Reactions (R1) and (R2) of 6×10^{-7} s⁻¹. The predicted product of (R2), (CH₃)₂C(OH)O, would decompose to form acetic acid (CH₃C(O)OH), and CH₃ radicals which are converted to HO₂ and HCHO. Following the well-characterised degradation of HCHO into HO₂ the overall result of (R1) initiated acetone degradation is therefore HO_x production (net +0.6 HO_x per CH₃C(O)CH₃ destroyed, assuming UT chemistry not NO limited). The loss of acetone via (R1–R2) was thus predicted to compete with photolysis (R3, net + 3.2 HO_x) and reaction with OH (R4, net +1.2 HO_x).



Large uncertainties remain however, and it is unclear which of (R1), (R3) or (R4) is the principal process for CH₃C(O)CH₃ degradation, and subsequent radical production in the UT. Whilst $k_4(T)$ values are reasonably well-established (Wollenhaupt et al., 2000), the Reaction (R3) photolysis quantum yields recently reported by Blitz et al. (2004) are considerably smaller than earlier measurements (Gierczak et al., 1998); the discrepancy is particularly large (\approx an order of magnitude) at the low temperatures of the UT. Meanwhile CH₃C(O)CH₃ degradation via (R1) has yet to be experimentally verified, and theoretical estimates for the equilibrium constant K_1 (the crucial parameter for assessing atmospheric impact) differ widely. In a second publication (Hermans et al., 2005) demonstrated that their calculations reproduced experimental results for the analogous reactions of HO₂ with HCHO (Veyret et al., 1989) and CH₃CHO (Tomas et al., 2001). Hermans et al. (2005) nonetheless acknowledged that their predictions for (R1) still await experimental verification. From thermochemical calculations (Benson, 2001) had previously identified a stepwise addition and rearrangement mechanism for (R1), with the group additivity method used to estimate a

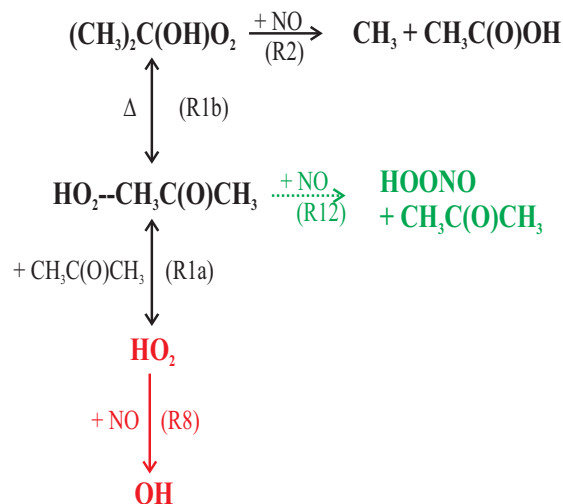


Fig. 1. Depiction of the chemistry described in this manuscript. Reaction with NO (R8, in red) was used to convert HO₂ to OH for detection by LIF in these laboratory experiments (Sect. 2.1). Competition from HO₂ + CH₃C(O)CH₃ leads to reduced OH yields, from which kinetic and thermodynamic parameters for (R1) were derived (see Sect. 3.1). Note: these experiments did not differentiate between the reactions of atmospheric interest (R1–R2, in black) and an alternative removal path for HO₂ (R1a followed by R12, in green), important only in the laboratory.

value of $K_1(298 \text{ K}) = 3.2 \times 10^{-19}$ cm³ molecule⁻¹, nearly two orders of magnitude smaller than reported by Hermans et al. (2004). Cours et al. (2007) used quantum-chemical methods to calculate different (from Hermans) intermolecular geometries for the HO₂--CH₃C(O)CH₃ complex, considerably smaller forward rate-coefficients ($k_1(200\text{--}298 \text{ K}) \approx 3 \times 10^{-16}$ cm³ molecule⁻¹ s⁻¹), and consequently small values for K_1 at around $T = 210$ K to indicate that (R1) has no atmospheric relevance. Whilst differing in important details, the results of all three studies indicate that HO₂--CH₃C(O)CH₃ interactions are inefficient at around $T = 298$ K, in agreement with the only available laboratory investigation by Gierczak and Ravishankara (2000), who reported $k(298 \text{ K}) < 8 \times 10^{-16}$ cm³ molecule⁻¹ s⁻¹. The work presented in this manuscript details the first laboratory studies to investigate HO₂--CH₃C(O)CH₃ interactions at low temperatures characteristic of the tropopause, together with new theoretical calculations on the (R1) equilibrium. The potential for (R1) to impact on the chemistry of the upper-troposphere was assessed in a global 3-D chemical model.

2 Methods

Sections 2.1 and 2.2 below present respectively the experimental and the atmospheric modeling methods used in this work. Details of the quantum chemical methodology used to

assess the uncertainties in $K_1(T)$ are presented in the Supplement.

2.1 Laboratory experiments

The experiments detailed in this work used Pulsed Laser Photolysis (PLP) reaction initiation coupled to pulsed Laser Induced Fluorescence (LIF) detection of OH. The experimental set-up has been published previously (Wollenhaupt et al., 2000; Dillon et al., 2006), and is described only briefly here. Experiments were conducted in a 500 cm³ jacketed quartz reactor. Temperature was controlled by the circulation of a cryogenic fluid through the outer jacket, and monitored with a J-type thermocouple to an estimated accuracy of ± 2 K. Reaction was initiated by an excimer laser operating at 351 nm (XeF). The frequency-doubled emission from a Nd-YAG pumped dye laser was used to excite the $A^2\Sigma(v=1) \leftarrow X^2\Pi(v=0)$, $Q_{11}(1)$ transition of OH at 281.997 nm. The resulting fluorescence from OH was detected by a photomultiplier tube, which was shielded by 309 ± 5 nm interference and BG 26 (glass cut-off) filters.

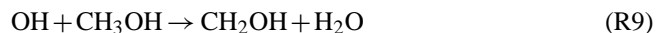
HO₂ was generated following 351 nm photolysis of Cl₂ using well-established Cl-atom chemistry (R5–R7). Laser fluences of ≈ 8 mJ cm⁻² were used in conjunction with $[Cl_2] = 1 \times 10^{14}$ molecule cm⁻³ to generate an estimated initial chlorine atom concentration of $[Cl] \sim 5 \times 10^{11}$ molecule cm⁻³.



Reagent concentrations, typically $[CH_3OH] = 5 \times 10^{14}$ and $[O_2] = 4 \times 10^{16}$ molecule cm⁻³ were chosen such that Cl was converted within 50 μ s and at 97 % yield to HO₂. These experiments did not employ direct HO₂ detection, but relied on its conversion to OH by the presence of NO at concentrations of $(1-3) \times 10^{14}$ molecule cm⁻³.



In the absence of CH₃C(O)CH₃, the observed LIF profiles were therefore characterised by the formation of OH (R8, ≈ 1 ms) followed by its slow decay via (R4) and (R9–R10).



CH₃C(O)CH₃ was added in concentrations of up to 1.6×10^{15} molecule cm⁻³ to this photolysis mixture. The competition (see Fig. 1) between CH₃C(O)CH₃ and NO for reaction with HO₂, and the impact upon observed yields of OH, was used to derive kinetic parameters for (R1). Analysis of these experimental OH profiles was assisted by use of numerical simulation using the FACSIMILE program (Curtis and Sweetenham, 1987) using an appropriate chemical scheme (see Sect. 3.1.2).

Precursor concentrations were determined optically by absorption at $\lambda = 184.9$ nm in a 43.8 cm absorption cell located downstream of the reactor (Dillon et al., 2005). Literature values for $\sigma_{185\text{nm}}(CH_3C(O)CH_3) = 3.01 \times 10^{-18}$ cm² molecule⁻¹ (Gierczak et al., 2003) and $\sigma_{185\text{nm}}(CH_3OH) = 6.65 \times 10^{-19}$ cm² molecule⁻¹ (Dillon et al., 2005) were used to determine $[CH_3C(O)CH_3]$ and $[CH_3OH]$ via the Beer-Lambert law. Values of $[NO]$, $[Cl_2]$, $[O_2]$ and $[N_2]$ were calculated to an estimated accuracy of ± 15 % from bulb or cylinder partial-pressures, calibrated mass-flow rates and measurements of T and P . Total gas flow rates of 500–1000 cm³ (STP) min⁻¹ ensured that a fresh gas sample was available for photolysis at each pulse.

Chemicals: liquid samples of CH₃C(O)CH₃ (Merck > 99.8 %) and CH₃OH (LS Labor > 99.8 %) were subject to repeated freeze-pump-thaw cycles; NO (Linde) was distilled by repeatedly removing the light boiling fractions at 77 K and discarding the frozen residue as the sample warmed; N₂ and O₂ (Messer 5.0, 99.999 %), and Cl₂ (Linde 2.0 % in He) were used as supplied.

2.2 Atmospheric modelling

The general circulation model for atmospheric chemistry ECHAM5/MESSy1 (henceforth EMAC), (Jöckel et al., 2005, 2006) was used to investigate the impact of (R1), with particular focus upon CH₃C(O)CH₃ degradation and CH₃C(O)O₂H formation. EMAC was used with T42 spectral resolution, corresponding to $2.8^\circ \times 2.8^\circ$ at the surface. The vertical resolution was 90 layers, of which about 25 were located in the troposphere. The model dynamics was weakly nudged (Jeuken et al., 1996; Lelieveld et al., 2007) towards the analysis data of the ECMWF operational model (up to 100 hPa) in order to realistically represent meteorology in the troposphere. Important changes were made to the model to account for recent improvements in the kinetic/photochemical database for reactions of CH₃C(O)CH₃ and CH₃C(O)OH. Quantum yields for CH₃C(O)CH₃ photolysis were based on results from Blitz et al. (2004) as preferred by IUPAC (Atkinson et al., 2006). In addition, rate coefficients for CH₃C(O)OH formation and loss processes were updated (see Table 1) to reflect recent laboratory data on the reaction of HO₂ with acetylperoxy radicals (Hasson et al., 2004; Dillon and Crowley, 2008; Jenkin et al., 2008) and several recent studies of the OH + CH₃C(O)OH reaction, see IUPAC (2011) and references therein.

3 Results and discussion

Section 3.1 details the results from the laser-kinetic laboratory-based study of (R1), including derivations of a lower-limiting forward rate coefficient at $T = 207$ K. In Sect. 3.2 we present a discussion of the sensitivity of these experiments and calculations. Section 3.3 details results

Table 1. Modifications to the chemical scheme used in the modelling studies.

Reactions included in SR1 (& SR2):	k^*
$\text{CH}_3\text{C}(\text{O})\text{OH} + \text{OH} \rightarrow \text{CH}_3\text{O}_2$	$4.0 \times 10^{-14} \exp(850/T)$
$\text{CH}_3\text{C}(\text{O})\text{O}_2 + \text{HO}_2 \rightarrow \text{CH}_3\text{C}(\text{O})\text{O}_2\text{H}$	$0.41 \times 5.2 \times 10^{-13} \exp(980/T)$
$\text{CH}_3\text{C}(\text{O})\text{O}_2 + \text{HO}_2 \rightarrow \text{CH}_3\text{C}(\text{O})\text{OH}$	$0.15 \times 5.2 \times 10^{-13} \exp(980/T)$
$\text{CH}_3\text{C}(\text{O})\text{O}_2 + \text{HO}_2 \rightarrow \text{CH}_3\text{O}_2 + \text{OH}$	$0.44 \times 5.2 \times 10^{-13} \exp(980/T)$
$\text{CH}_3\text{C}(\text{O})\text{O}_2 + \text{CH}_3\text{O}_2 \rightarrow \text{HCHO} + \text{HO}_2 + \text{CH}_3\text{O}_2$	$0.9 \times 2 \times 10^{-12} \exp(500/T)$
$\text{CH}_3\text{C}(\text{O})\text{O}_2 + \text{CH}_3\text{O}_2 \rightarrow \text{CH}_3\text{C}(\text{O})\text{OH} + \text{HCHO}$	$0.1 \times 2 \times 10^{-12} \exp(500/T)$
$\text{CH}_3\text{C}(\text{O})\text{O}_2 + \text{C}_2\text{H}_5\text{O}_2 \rightarrow 0.82\text{CH}_3\text{O}_2 + \text{CH}_3\text{CHO} + 0.82 \text{HO}_2 + 0.18 \text{CH}_3\text{C}(\text{O})\text{OH}$	$4.4 \times 10^{-13} \exp(1070/T)$
Reactions only included in SR2:	
$\text{HO}_2 + \text{CH}_3\text{C}(\text{O})\text{CH}_3 \rightarrow (\text{CH}_3)_2\text{C}(\text{OH})\text{OO} \text{ (R1)}$	$5.1 \times 10^{-15} \exp(1335./T)$
$(\text{CH}_3)_2\text{C}(\text{OH})\text{OO} \rightarrow \text{HO}_2 + \text{CH}_3\text{C}(\text{O})\text{CH}_3 \text{ (R-1)}$	$6.5 \times 10^{12} \exp(-4750/T) \text{ s}^{-1}$
$(\text{CH}_3)_2\text{C}(\text{OH})\text{OO} + \text{NO} \rightarrow \text{CH}_3\text{O}_2 + \text{CH}_3\text{C}(\text{O})\text{OH} + \text{NO}_2 \text{ (R2)}$	$2.7 \times 10^{-12} \exp(360/T)$
$(\text{CH}_3)_2\text{C}(\text{OH})\text{OO} + \text{HO}_2 \rightarrow (\text{CH}_3)_2\text{C}(\text{OH})\text{OOH} + \text{O}_2 \text{ (R13)}$	4×10^{-11}

* k in units of $\text{cm}^3 \text{ molecule}^{-1} \text{ s}^{-1}$ unless stated otherwise; values taken from the IUPAC evaluations of Atkinson et al. (2004, 2006) and (for SR2) Hermans et al. (2004).

from incorporation of the largest published (Hermans et al., 2004) values for $k_1(T)$ and $K_1(T)$ into a global 3-D chemical model.

3.1 Results from laboratory studies

Evidence for reaction was only observed at the lowest temperatures. Fairly complex chemistry controlled the OH production and loss depicted in the OH profiles. Numerical simulations (see Sects. 3.1.2–3.1.3 below) were therefore used to obtain best estimates for experimentally derived rate ($k_{1\text{exp}}$) and equilibrium ($K_{1\text{exp}}$) constants, and to identify these quantities with either HO₂–CH₃C(O)CH₃ complex formation (R1a) or the overall (R1) process.

3.1.1 Evidence for reaction between HO₂ and CH₃C(O)CH₃ at $T < 230 \text{ K}$

In back-to-back experiments where unchanged reagent concentrations and laser fluences were used, time-resolved OH LIF profiles were recorded prior to and following the addition of CH₃C(O)CH₃. Figure 2 displays a pair of typical profiles recorded following generation of HO₂ (R5–R7) in the presence of excess [NO] = $1.5 \times 10^{14} \text{ molecule cm}^{-3}$ at $T = 207 \text{ K}$. In the absence of CH₃C(O)CH₃ (square datapoints), OH was formed on a timescale ($\approx 500 \mu\text{s}$) consistent with the kinetics of HO₂ + NO (R8). The circles were recorded following addition of [CH₃C(O)CH₃] = $7.5 \times 10^{14} \text{ molecule cm}^{-3}$, and are characterised by a dramatic reduction in the OH LIF signal. Such a change in OH makes sense if CH₃C(O)CH₃ efficiently competes for the HO₂, so reducing the amount available for conversion (R8) to OH. There are however a number of physical and chemical processes by which CH₃C(O)CH₃ may perturb the LIF signal in these experiments; these must be isolated from the

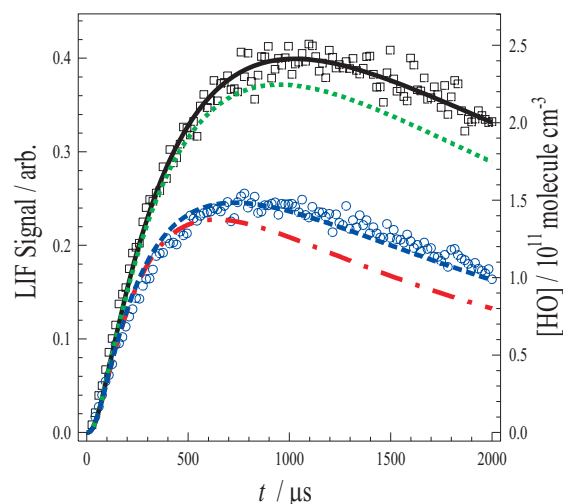


Fig. 2. OH LIF profiles recorded following HO₂ generation (R5–R7) in the presence of NO ($1.5 \times 10^{14} \text{ molecule cm}^{-3}$) at 207 K and 25 Torr. Black squares are data with [CH₃C(O)CH₃] = 0; the black solid line is the numerical simulation used to calibrate the LIF signal response. Blue circles are datapoints with [CH₃C(O)CH₃] = $7.5 \times 10^{14} \text{ molecule cm}^{-3}$, and are associated with three numerical simulations: simulation using published theoretical values of k_1 and K_1 from (Hermans et al., 2004) are depicted as the red dot-dashed line; the green dotted line represents $k_1 = 0$; the blue dashed line represents a simulation using $k_{-1} = 0$ and a forward rate coefficient $k_1(207 \text{ K}) = 2 \times 10^{-12} \text{ cm}^3 \text{ molecule}^{-1} \text{ s}^{-1}$.

impact of (R1–R2) if we are to obtain a reasonable estimate for the efficiency of the HO₂–CH₃C(O)CH₃ interaction.

The effect of CH₃C(O)CH₃ upon physical processes was assessed previously (Dillon and Crowley, 2008). No changes to LIF intensity were observed following

addition of CH₃C(O)CH₃ at concentrations up to 4×10^{15} molecule cm⁻³, demonstrating that changes to fluorescence yields and/or detection efficiency of OH were negligible. The changes in LIF signal observed in Fig. 2 therefore directly reflect changes to OH production and loss chemistry due to CH₃C(O)CH₃. Other parameters such as photolysis/probe laser fluence and reagent concentrations were unchanged. Data obtained in the absence of CH₃C(O)CH₃ may thus be used to calibrate the experiment.

A semi-quantitative analysis of the data presented in Fig. 2 may be made by consideration of first-order rate constants for HO₂ removal (assumed equivalent to the observed OH formation rate) and ignoring the thermal decomposition of the product peroxy radical (setting $k_{-1} = 0$). In the absence of CH₃C(O)CH₃, HO₂ is removed by reaction with NO at a rate of $k_8[\text{NO}] = 2000 \text{ s}^{-1}$ (uses $k_8(200\text{--}400 \text{ K}) = 3.45 \times 10^{-12} \exp(270/T) \text{ cm}^3 \text{ molecule}^{-1} \text{ s}^{-1}$ (Atkinson et al., 2004)). As a first approximation we attribute all of the reduction in observed OH ($\approx 40\%$) to the impact of CH₃C(O)CH₃ via (R1). To compete with (R8), the CH₃C(O)CH₃ must sequester HO₂ at a rate given by $k_{1\text{exp}}[\text{CH}_3\text{C(O)CH}_3]$ of several hundreds persecond, implying that $k_{1\text{exp}}(207 \text{ K}) > 1 \times 10^{-12} \text{ cm}^3 \text{ molecule}^{-1} \text{ s}^{-1}$. A series of such back-to-back experiments was conducted, and the LIF signals observed were in inverse proportion to [CH₃C(O)CH₃], indicating that this result is robust. Details of the experimental conditions used in these and other experiments are listed in Table 2. Note that an exact analytical treatment of these datasets was not appropriate, as OH production did not commence at $t = 0$ (there is a short delay whilst the precursor HO₂ is generated).

Experiments conducted at somewhat higher temperatures were characterised by much smaller changes in OH. For example, Fig. 3 displays a typical pair of OH profiles obtained at $T = 228 \text{ K}$, wherein the addition of [CH₃C(O)CH₃] = 1×10^{15} molecule cm⁻³ resulted in an approximate 15% reduction in LIF intensity. Whilst some of this change in OH could be due to (R1), the addition of CH₃C(O)CH₃ to the reaction mixtures does impact on OH via other chemical processes, e.g. by removing OH directly (R4), or the precursor Cl radicals in (R11).



In summary, the observations presented in Figs. 2–3 provide some evidence for the theoretical predictions of Hermans et al. (2004) of a significant forward rate coefficient with $k_1(200\text{--}210 \text{ K}) \approx 3 \times 10^{-12} \text{ cm}^3 \text{ molecule}^{-1} \text{ s}^{-1}$ and a strongly temperature dependent reverse process (R1). The lower limiting forward rate coefficient is clearly not consistent with the much smaller $k_1 \sim 10^{-16} \text{ cm}^3 \text{ molecule}^{-1} \text{ s}^{-1}$ predicted by Cours et al. (2007). To isolate and quantify the effects on observed OH that were attributable to (R1), and hence better constrain our estimates of k and K , numerical simulations of the datasets were conducted.

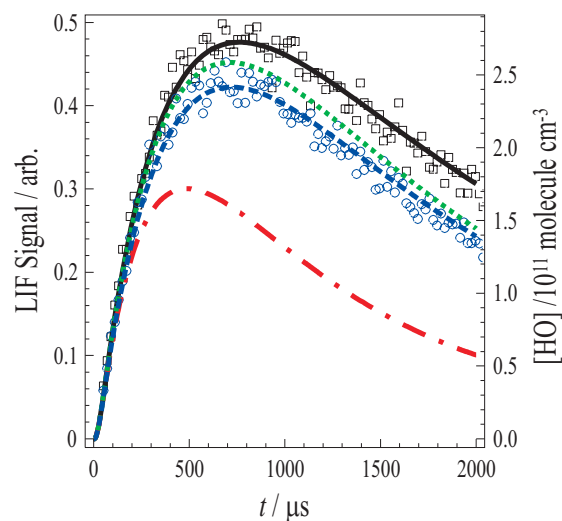


Fig. 3. OH LIF profiles recorded following HO₂ generation in the presence of NO (1.6×10^{14} molecule cm⁻³) at 228 K and 85 Torr. Black square datapoints were obtained with [CH₃C(O)CH₃] = 0; the black solid line is the associated numerical simulation used to calibrate the LIF signal response. Blue circles depict data obtained at [CH₃C(O)CH₃] = 1.0×10^{15} molecule cm⁻³ and are associated with three numerical simulations. Results from simulations using theoretical values of k_1 and k_{-1} from Hermans et al. are depicted as the red dot-dashed line. The green dotted line represents $k_1 = 0$ (indistinguishable from simulations using parameters from, Cours et al., 2007). As indicated by the blue dashed line, the data could be reasonably well reproduced using much smaller values of K_1 (see Sect. 3.1.2).

3.1.2 Numerical simulations of the (R1) data

Numerical simulation of kinetic data using the FACSIMILE program (Curtis and Sweetenham, 1987) was used to assess the reactions of CH₃C(O)CH₃ with the radicals Cl, HO₂ and OH. Experimentally determined values of P , T , [CH₃C(O)CH₃], [CH₃OH], [NO], [O₂], [Cl₂], together with calculated [Cl] were used to initialise the simulations. Table 3 lists the reactions and rate coefficients used to simulate the kinetic behaviour of [Cl], [HO₂], [OH] and [(CH₃)₂C(OH)OO]. The first task was to simulate the simple chemistry that occurs in the absence of CH₃C(O)CH₃. The results of one such simulation are displayed as the black, solid line passing through the square datapoints on Fig. 2. The OH production and loss processes are reasonably well-characterised, and these datasets obtained in the absence of CH₃C(O)CH₃ were therefore used to define the LIF sensitivity (fixing the relative positions of the LIF and [OH] y-axes on Fig. 2). The impact of any non-(R1) related effects of adding CH₃C(O)CH₃ may be identified in simulations using $k_1 = 0$ (the green dotted line on Fig. 2). This simulation (indistinguishable from simulations using values of k_1 and K_1 from Cours et al., 2007) clearly underestimates the impact of [CH₃C(O)CH₃] = 1×10^{15} molecule cm⁻³ on the

Table 2. Experimental conditions and estimated $k_{1\text{exp}}$ and $K_{1\text{exp}}$ parameters.

T/K	P/Torr	$[\text{CH}_3\text{OH}]^{\text{a}}$	$[\text{NO}]^{\text{a}}$	$[\text{O}_2]^{\text{a}}$	$[\text{CH}_3\text{C}(\text{O})\text{CH}_3]^{\text{a}}$	n^{b}	$k_{1\text{exp}}^{\text{c}}$	$K_{1\text{exp}}$
207	25	4.7	1.5	440	0, 0.9–7.5	7	2.0	n/a
210	25	4.6	1.5	430	0, 0.6–7.4	8	1.3	83
215	25	4.5	1.4	420	0, 1.8–7.1	6	0.7	59
220	85	8.2	1.4	570	0, 4.4–16.2	5	0.4	19
228	85	10.0	2.4	530	0, 4.9–17.2	6	<0.2	7.5
235	85	16	2.6	900	0, 2.9–14.5	5	n/a	n/a
273	85	17	3.3	450	0, 2.6–12.4	6	n/a	n/a
298	85	16	3.0	410	0, 2.4–11.3	6	n/a	n/a

^a all reagent concentrations in units of 10^{14} molecule cm^{-3} ; ^b n = number of experiments at different $[\text{CH}_3\text{C}(\text{O})\text{CH}_3]$; ^c lower limits to $k_{1\text{exp}}/10^{-12}$ cm^3 molecule⁻¹ s⁻¹ calculated assuming $k_{-1} = 0$; $K_{1\text{exp}}$ in units of 10^{-17} cm^3 molecule⁻¹ estimates obtained by numerical simulation (see Sect. 3.1.3 for details).

observed OH profile (the blue circles), suggesting a good experimental sensitivity, and that $\text{CH}_3\text{C}(\text{O})\text{CH}_3$ does indeed interact strongly with HO_2 at this temperature. Note that the small differences in the simulations with $[\text{CH}_3\text{C}(\text{O})\text{CH}_3] = 0$ (black solid line), and the $k_1 = 0$ green, dotted line were principally due to an increased OH removal rate via reaction with the added acetone (R4), and to a lesser extent scavenging of the Cl precursor (R11).

Data simulations incorporating (R1) chemistry (see Fig. 1) were less straightforward, with three crucial parameters $k_1(T)$, $K_1(T)$ and $k_2(T)$ to be estimated for simulation at each experimental temperature (207–298 K). There are to date no theoretical or experimental studies of (R2), $(\text{CH}_3)_2\text{C}(\text{OH})\text{OO} + \text{NO}$, in the literature. In this work, we have therefore adopted the expression $k_2(200\text{--}300\text{ K}) = 2.7 \times 10^{-12} \exp(360/T)$, listed by Atkinson et al. (2004) for the reaction of NO with another C₃ peroxy radical, $\text{CH}_3\text{CH}(\text{O}_2)\text{CH}_3$. For the simulations presented in Fig. 2 this expression gives $k_2(207\text{ K}) = 1.5 \times 10^{-11}$ cm^3 molecule⁻¹ s⁻¹, which as Hermans et al. (2004) noted is the value reported for a number of peroxy + NO reactions at around $T = 200\text{ K}$. Initial values of $k_1(207\text{ K}) = 3.2 \times 10^{-12}$ cm^3 molecule⁻¹ s⁻¹ and $K_1(207\text{ K}) = 9.1 \times 10^{-13}$ cm^3 molecule⁻¹ were taken from the calculations of Hermans et al. (2004). The resulting simulation of the data in Fig. 2 is displayed as the red, dot-dashed line. This simulation slightly overestimates the impact of $\text{CH}_3\text{C}(\text{O})\text{CH}_3$ on the observed OH (blue circle datapoints). A lower-limit $k_{1\text{exp}}(207\text{ K}) > 2 \times 10^{-12}$ cm^3 molecule⁻¹ s⁻¹ was obtained from a series of similar such simulations of all the $T = 207\text{ K}$ data in which the dissociation process (R1) was neglected. This and similar experimentally derived lower limiting values of $k_{1\text{exp}}(T)$ are listed in Table 2.

A similar methodology was used to simulate the $T = 228\text{ K}$ data displayed in Fig. 3. In contrast to results obtained at lower T , there is little difference between the data obtained without $\text{CH}_3\text{C}(\text{O})\text{CH}_3$ (black squares), and at $[\text{CH}_3\text{C}(\text{O})\text{CH}_3] = 1.0 \times 10^{15}$ molecule cm^{-3} (blue circles).

The black, solid line again represents a simulation with $[\text{CH}_3\text{C}(\text{O})\text{CH}_3] = 0$, which reproduced the experimental data well and was therefore used to fix the relative positions of the LIF and [OH] y-axes. The results obtained in the presence of $\text{CH}_3\text{C}(\text{O})\text{CH}_3$ at $T = 228\text{ K}$ could be simulated reasonably well using $k_{1\text{exp}} = 0$ (e.g. the green dotted line on Fig. 3), demonstrating that within the experimental scatter, little or no interaction between HO_2 and $\text{CH}_3\text{C}(\text{O})\text{CH}_3$ was evident. Similar results were obtained at all higher temperatures (see Table 2), in line with the earlier experimental study by Gierczak and Ravishankara (2000) who observed no reactive loss of HO_2 in the presence of $\text{CH}_3\text{C}(\text{O})\text{CH}_3$ at 298 K.

In an investigation such as this, where numerical simulations were used to analyse the experimental data, there were several potential sources of error. Systematic uncertainties, both experimental and from the literature/estimated rate coefficients used for simulations almost certainly outweigh any experimental scatter (see Figs. 2–3). We estimate that important contributions derive from uncertainties (2σ) in the following parameters: $\pm 5\%$ in $[\text{CH}_3\text{C}(\text{O})\text{CH}_3]$; $\pm 15\%$ in $[\text{NO}]$; $\pm 2\text{ K}$ in T ; $\pm 50\%$ in k_2 ; $\pm 20\%$ in k_8 . Propagation of these potential sources of error does not however allow us to reconcile the observed OH profiles with the theoretical predictions of Hermans et al. for the overall (R1) process (see e.g. the red dot-dash line on Fig. 3). Different chemical scenarios were therefore considered in an attempt to explain the experimental observations, and identify the processes involved (R1 or just R1a).

3.1.3 Simulations varying $k_1(T)$, $K_1(T)$ and $k_2(T)$

Simulations using FACSIMILE were constructed whereby different values of $k_1(T)$, $K_1(T)$ and $k_2(T)$ could be tested alongside the basis set of reactions listed in Table 3. As regards k_1 , some constraint is provided by the lower-limit obtained at $T = 207\text{ K}$. Considerably smaller values of k_1 were required to adequately simulate the data at higher temperatures if Hermans $K_1(T)$ was used. At $T = 228\text{ K}$ for

Table 3. Chemistry used in numerical simulations (Sect. 3.1.2).

Reaction	k^a	Ref. ^b
Basic chemistry (used in all simulations):		
Cl + CH ₃ OH → CH ₂ OH + HCl (R6)	$1.4 \times 10^{-10} \exp(-280/T)$	
Cl + CH ₃ C(O)CH ₃ → CH ₂ C(O)CH ₃ + HCl (R11)	$1.5 \times 10^{-11} \exp(-590/T)$	
CH ₂ OH + O ₂ → HCHO + HO ₂ (R7)	$5.6 \times 10^{-9} \exp(-1700/T)$	Nesbitt et al. (1988)
CH ₂ OH + Cl ₂ → Cl + ClCH ₂ OH	2.7×10^{-11}	
NO + HO ₂ → OH + NO ₂ (R8)	$3.6 \times 10^{-12} \exp(270/T)$	
HO ₂ + HO ₂ → H ₂ O ₂ + O ₂	$2.2 \times 10^{-13} \exp(600/T) + 1.9 \times 10^{-33} [\text{M}] \exp(980/T)$	
HO ₂ + CH ₃ OH → HO ₂ ·CH ₃ OH	$2.8 \times 10^{-15} \exp(1800/T)$	Christensen et al. (2006)
HO ₂ ·CH ₃ OH → HO ₂ + CH ₃ OH	$1.15 \times 10^{10} \exp(-2698/T)$	Christensen et al. (2006)
OH + CH ₃ OH → CH ₂ OH + H ₂ O (R9a)	$0.85 \times 6.67 \times 10^{-18} T^2 \exp(140/T)$	Dillon et al. (2005)
OH + CH ₃ OH → CH ₃ O + H ₂ O (R9b)	$0.15 \times 6.67 \times 10^{-18} T^2 \exp(140/T)$	Dillon et al. (2005)
OH + CH ₃ C(O)CH ₃ → CH ₂ C(O)CH ₃ + H ₂ O (R4)	$8.8 \times 10^{-12} \exp(-1320/T) + 1.7 \times 10^{-14} \exp(423/T)$	
OH + NO + M → HONO + M (R10)	$k_0 = 7.4 \times 10^{-31} (T/300)^{-2.4} [\text{N}_2], k_\infty = 3.3 \times 10^{-11} (T/300)^{-0.3}; F_c = 0.81$	
OH + HO ₂ → H ₂ O + O ₂	$4.8 \times 10^{-11} \exp(250/T)$	
CH ₂ C(O)CH ₃ + O ₂ → O ₂ CH ₂ C(O)CH ₃	$7.2 \times 10^{-13} \exp(130/T)$	
O ₂ CH ₂ C(O)CH ₃ + NO → OCH ₂ C(O)CH ₃	$2.8 \times 10^{-12} \exp(300/T)$	
OCH ₂ C(O)CH ₃ → CH ₃ CO + HCHO	$\geq 5 \times 10^7 \text{ s}^{-1}$	Orlando et al. (2000)
CH ₃ CO + O ₂ → CH ₃ C(O)O ₂	$0.95 \times 5.1 \times 10^{-12}$ at around $T = 213 \text{ K}$	Carr et al. (2011)
CH ₃ CO + O ₂ → OH	$0.05 \times 5.1 \times 10^{-12}$ at around $T = 213 \text{ K}$	Carr et al. (2011)
CH ₃ CO + Cl ₂ → CH ₃ C(O)Cl + Cl	$2.8 \times 10^{-11} \exp(-47/T)$	Maricq and Szente (1996)
CH ₃ C(O)O ₂ + NO → CH ₃ + CO ₂ + NO ₂	$7.5 \times 10^{-12} \exp(290/T)$	
CH ₃ + O ₂ + M → CH ₃ O ₂ + M	$k_0 = 1 \times 10^{-30} (T/300)^{-3.3} [\text{N}_2], k_\infty = 1.8 \times 10^{-12} (T/300)^{1.1}$	
CH ₃ + Cl ₂ → CH ₃ Cl + Cl	$4.79 \times 10^{-12} \exp(-240/T)$	Timonen (1988)
CH ₃ O ₂ + NO → CH ₃ O + NO ₂	$2.3 \times 10^{-12} \exp(360/T)$	
CH ₃ O + O ₂ → HO ₂ + HCHO	1.9×10^{-15}	
CH ₃ O + NO → HNO + HCHO	$2.3 \times 10^{-12} (T/300)^{-0.7}$	
CH ₃ O + NO + M → CH ₃ ONO + M	$2.6 \times 10^{-29} (T/300)^{-2.8} [\text{M}]$	
(R1) and related chemistry		
HO ₂ + CH ₃ C(O)CH ₃ → (CH ₃) ₂ C(OH)OO (R1)	$k_1(T)$, varied	This work
(CH ₃) ₂ C(OH)OO → HO ₂ + CH ₃ C(O)CH ₃ (R1)	$k_{-1}(T)$, varied	This work
(CH ₃) ₂ C(OH)OO + NO → CH ₃ + CH ₃ C(O)OH + NO ₂ (R2)	$k_2(T), 2.7 \times 10^{-12} \exp(360/T)$, varied	estimate, see Sect. 3.1.2
(CH ₃) ₂ C(OH)OO + HO ₂ → (CH ₃) ₂ C(OH)OOH + O ₂ (R13)	4×10^{-11}	estimate
HO ₂ + CH ₃ C(O)CH ₃ → HO ₂ ·CH ₃ C(O)CH ₃ (R1a)	$k_{1a}(T)$, varied, see Sect. 3.1.3	Aloisio and Francisco (2000) and Hermans et al. (2005)
HO ₂ ·CH ₃ C(O)CH ₃ → HO ₂ + CH ₃ C(O)CH ₃ (R1a)	$k_{-1a}(T)$, varied, see Sect. 3.1.3	Aloisio and Francisco (2000) and Hermans et al. (2005)
HO ₂ ·CH ₃ C(O)CH ₃ + NO → CH ₃ C(O)CH ₃ + HOONO (R12)	$k_{12}(T), 2.7 \times 10^{-12} \exp(360/T)$, varied	estimate, see Sect. 3.1.3

^a k in units of $\text{cm}^3 \text{ molecule}^{-1} \text{ s}^{-1}$ unless stated otherwise; ^b values taken from (IUPAC, 2011) unless stated otherwise.

example, a reasonable reproduction of the data was obtained using $k_{1\text{exp}} = 0$ (green, dotted line in Fig. 3), or up to $4 \times 10^{-13} \text{ cm}^3 \text{ molecule}^{-1} \text{ s}^{-1}$. Such a strong temperature dependence for the forward association process does not seem reasonable. The temperature dependence of an equilibrium constant for such an association reaction is usually dominated by the barrier to the dissociation process (e.g. R1). All experimental datasets were therefore simulated using $k_1(T) = 3.3 \times 10^{-15} \exp(1335/T) \text{ cm}^3 \text{ molecule}^{-1} \text{ s}^{-1}$ from Hermans et al. (2004) with the pre-exponential factor scaled to yield our lower limit value of $k_{1\text{exp}} = 2 \times 10^{-12} \text{ cm}^3 \text{ molecule}^{-1} \text{ s}^{-1}$ at 207 K. Simulations using

these constrained values of k_1 , and varying k_2 within generous uncertainty limits of up to a factor of three were not able to reproduce the $T = 228 \text{ K}$ data. In practice therefore, orders-of-magnitude larger values of k_{-1} were required to adequately reproduce the experimental observations.

Experimentally constrained estimates of $K_{1\text{exp}}(T)$ were obtained by using the normalised upper-limit values of $k_1(T)$, $k_2(T) = 2.7 \times 10^{-12} \exp(360/T)$ as described above, and by manually adjusting k_{-1} until the data at $T = 210, 215, 220$ and 228 K was best produced by simulation. For example, the dashed blue line on Fig. 3 represents a reasonable reproduction of a $T = 228 \text{ K}$ dataset (the

blue circles) using $k_1 = 1.1 \times 10^{-12} \text{ cm}^3 \text{ molecule}^{-1} \text{ s}^{-1}$, $k_2 = 1.3 \times 10^{-11} \text{ cm}^3 \text{ molecule}^{-1} \text{ s}^{-1}$ and a value for k_{-1} of 15000 s^{-1} . We can then calculate a value for the equilibrium constant of $K_{1\text{exp}}(228 \text{ K}) = k_{1\text{exp}}/k_{-1\text{exp}} = 7.5 \times 10^{-17} \text{ cm}^3 \text{ molecule}^{-1}$ via this method. It was possible to obtain values for the equilibrium constant at four temperatures below 230 K, which are listed in Table 2 and displayed in van't Hoff format in Fig. 4. Also displayed on Fig. 4 are lines representing $K_1(T)$ values from Hermans et al. (2004) and Cours et al. (2007), neither of which are well-reproduced by the results from this work. Striking however, is the coincidence of the equilibrium constants derived in this work, with the predictions for K_{1a} from Aloisio and Francisco (2004), and the recent experimental determinations from Grieman et al. (2011). The experiments presented in this work would be sensitive to K_{1a} if the forward reaction rate coefficient k_{1a} is similar to or greater than that used in the simulations, and if the resultant complexes can be irreversibly converted to other products. To address the first point, whilst there are no literature values for k_{1a} available, a rate coefficient of $k_{1a}(200\text{--}230 \text{ K}) \geq 2 \times 10^{-12} \text{ cm}^3 \text{ molecule}^{-1} \text{ s}^{-1}$ is reasonable for formation of such weakly bound complexes. By way of comparison Christensen et al. (2006) measured forward rate coefficients of around $1 \times 10^{-11} \text{ cm}^3 \text{ molecule}^{-1} \text{ s}^{-1}$ for the equivalent HO₂-CH₃OH complex at such temperatures, whilst a similarly large capture rate for OH by CH₃C(O)CH₃ was reported by Talukdar et al. (2003). Note also that at $T = 207 \text{ K}$, a forward rate coefficient of at least $2 \times 10^{-12} \text{ cm}^3 \text{ molecule}^{-1} \text{ s}^{-1}$ was determined in this work, and such processes are rarely, if ever, characterized by a strong temperature dependence. The complex is predicted to be short-lived, rapidly decomposing back to HO₂ + CH₃C(O)CH₃ (or indeed undergoing rearrangement (R1b) to the peroxy radical) such that, in these experiments, the only mechanism available for irreversible product formation would be by bimolecular reaction with one of the excess reagents. The complex is unlikely to interact with closed-shell molecules such as CH₃OH or CH₃C(O)CH₃, but given the predictions of a weakly bound terminal O-atom may react (R12) with the excess radical species NO.



The Reaction (R12) thus provides a means of removing HO₂ from the system, though in order to deplete OH in line with observation, the HOONO product should not decompose (to OH + NO₂) on our experimental timescales of milliseconds. A barrier of 83 kJ mol^{-1} for thermal decomposition of HOONO reported by Fry et al. (2004) does imply a sufficiently long lifetime for the HOONO at the temperature range (207–228 K) of interest in this work.

Estimates of K_{1a} derived from simulated OH profiles are inversely proportional to the value of k_{12} used to set up the simulation. Thus the values listed in Table 2 and depicted on Fig. 4 are only valid if (R12) proceeds (to non-OH products) at a similar rate to that reported for CH₃CH(O₂)CH₃ + NO

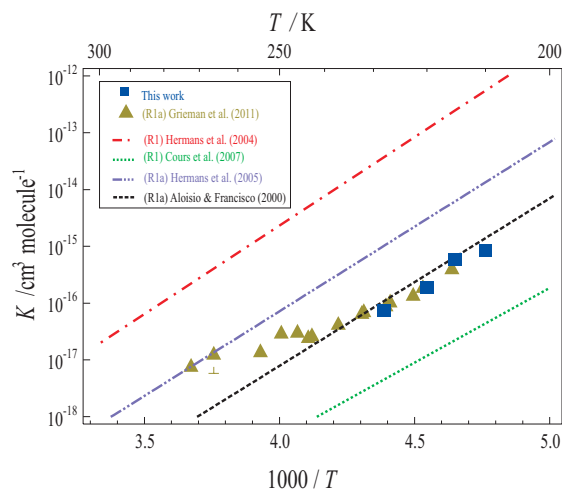


Fig. 4. van't Hoff plot used to compare determinations of K_1 (and K_{1a}). The red dot-dashed line and green dotted lines depict the (R1) results from Hermans et al. and Cours et al. respectively. Also displayed are results for (R1a): from Aloisio and Francisco (2000) $K_{1a}(200\text{--}300 \text{ K}) = 1.25 \times 10^{-29} \exp(6790/T) \text{ cm}^3 \text{ molecule}^{-1}$ (the black dashed line); from Hermans et al. (2005) $K_{1a}(200\text{--}300 \text{ K}) = 1.25 \times 10^{-29} \exp(7248/T) \text{ cm}^3 \text{ molecule}^{-1}$ (the purple dot-dashed line); and recent experimental results (green triangles) from Grieman et al. (2011). The blue square datapoints depict results from this work, which appear to describe $K_{1a}(T)$.

($k = 1.3 \times 10^{-11} \text{ cm}^3 \text{ molecule}^{-1} \text{ s}^{-1}$ at around 220 K). Whilst such simulations using (R12) adequately reproduced the size and shape of the observed OH profiles recorded at $T > 207 \text{ K}$, we note that no literature data is available for k_{12} . A necessarily detailed experimental or theoretical investigation of (R12) is beyond the scope of this manuscript. However, theoretical predictions of the geometry of the HO₂-CH₃C(O)CH₃ complex seem to indicate that access by NO to the radical oxygen site is not significantly sterically hindered. Furthermore, the dispersal of reaction energy of the HOONO formation across the entire acetone-HOONO complex can reduce the impact of prompt redissociation of the HOONO moiety. Hence k_{12} can be tentatively estimated to be comparable to that for the C3-RO₂ + NO reaction.

A “3rd Law” fit of the approximate K_{1a} values listed in Table 2, constrained by the calculated reaction entropy (Aloisio and Francisco, 2000; Hermans et al., 2005) yields $K_{1a}(215\text{--}228 \text{ K}) = 1.253 \times 10^{-29} \exp(6703/T)$. A tentative estimate of the enthalpy for complex formation is thus $\Delta H_{1a} = -55.7 \text{ kJ mol}^{-1}$. Taking into account merely systematic errors from the experiments (see Sect. 3.1.2 above) and a conservative $\pm 50\%$ in k_{12} we may similarly derive values in the range of -57.3 to $-54.2 \text{ kJ mol}^{-1}$ for ΔH_{1a} , indicating that the results derived here are in satisfactory agreement with the predictions of Aloisio and Francisco (2001) of $\Delta H_{1a} = -56.5 \text{ kJ mol}^{-1}$.

3.2 Discussion – sensitivity of experiments and theory

As was detailed in Sect. 3.1 above, the experimental observations from this work support predictions of Hermans et al. of an efficient HO₂-CH₃C(O)CH₃ interaction at low temperatures. Numerical simulations of the data however are consistent with complex formation (R1a) only, the first step in the postulated removal mechanism for atmospheric CH₃C(O)CH₃. No evidence was found in this work (or another recent experimental study from Grieman et al., 2011) for the subsequent rearrangement of the complex to form peroxy radicals (R1b). In this section we consider why sensitivity to (R1b) might have been lacking in these experiments.

3.2.1 Unknowns in the chemistry

Chemistry whereby HO₂, the HO₂-CH₃C(O)CH₃ complex or indeed other radical products are converted to OH would render the experiment blind to the reactions of interest, but it is difficult to assess the impact of such hitherto unknown reactions. It is worth noting that the experiments conducted at $T = 207$ K were characterised by large OH reductions upon CH₃C(O)CH₃ addition, indicating that such interferences were not dominant at this temperature.

Experimental concentrations of CH₃C(O)CH₃ and NO were chosen such that the overall rate of (R1) given by $k_1[\text{CH}_3\text{C}(\text{O})\text{CH}_3]$ was similar to, and could therefore impact on, the rate of NO converting HO₂ to OH (R8). Potential scavenging of the intermediate complex by NO was not anticipated. Good experimental sensitivity to the overall (R1) can only be obtained if the rearrangement (R1b) proceeds at a rate fast enough to compete with (R12) in addition to the thermal decomposition processes. This is certainly open to question, not least because of large uncertainties associated with k_{1a} , k_{1b} and k_{12} . The theoretical data allows estimation of the critical k_{1b} at the high pressure limit of ~ 270 s⁻¹ at 207 K and ~ 860 s⁻¹ at 220 K, using the CCSD(T)/aug-cc-pV ∞ Z//B3LYP data, while k_1 values from Hermans et al. (2004) may be combined with the experimental [CH₃C(O)CH₃] of up to 1.7×10^{15} molecule cm⁻³ to estimate an overall HO₂ loss of around 3000 s⁻¹ for (R1) at $T = 228$ K (data displayed in Fig. 2). This latter is then similar to the estimated (see Sect. 3.1.3 above) rate of scavenging of the complex by NO in (R12), which in turn is much faster than the thermal rearrangement of the H-bonded complex to the adduct. It is conceivable therefore that the experiments are only sensitive to K_{1a} because peroxy radical formation is too slow compared to competitive reactions. However, it is worth reiterating that the estimated rate constant (and products) of (R12) carry a large uncertainty also. Considerably lower NO concentrations characterise the UT, hence Reaction (R12) would not interfere with any adduct formation in the atmosphere.

3.2.2 Pressure effects

The published values of $k_1(T)$ from Hermans et al. (2004, 2005) are derived from transition state theory, and are consequently high-pressure limiting values. It is unclear whether the experiments from this work (e.g. $P = 85$ Torr (N₂) at 228 K) were conducted in conditions sufficiently close to the high-pressure limit. In the fall-off or low-pressure region, slower formation of the adduct leads to reduced experimental sensitivity. Again, this interference is important only in interpretation of laboratory data. The relevant parameter for atmospheric modelling is the equilibrium constant $K_1(T)$, itself unaffected by, for example, low pressures that would constrain stabilization of the complex or adduct, as well as the k_{-1} back dissociation reaction rates.

3.2.3 Uncertainties on the theoretical predictions

A third possible reason for the experiments insensitivity to (R1), namely that K_1 was itself overestimated by theory, has therefore more important implications for atmospheric chemistry. In new theoretical work, detailed here in the Supplement, we have conducted quantum chemical calculations on the complex (R1a) and subsequent adduct formation (R1b) from HO₂ + CH₃C(O)CH₃. Important results include that reaction enthalpies for complex formation (R1a) were fairly similar across all methodologies, as were barrier heights for adduct decomposition (R1b). Divergence was found however across different levels of theory for the overall adduct formation exothermicity (R1), or for the adduct formation energy barrier from the complex (R1b). The relative energy of the adduct with respect to the separated reactants reduces quite significantly upon increasing the basis set from double to triple zeta quality, on average by 4.3 kJ mol⁻¹. This implies a reduction in the $K_1(220$ K) of 1 order of magnitude; uncertainties of this order were already indicated by Hermans et al. Our current best level of theory available, CCSD(T)/aug-cc-pV ∞ Z//B3LYP/cc-pVTZ, suggests a well depth of 54.4 kJ mol⁻¹, 4.2 kJ mol⁻¹ below the best G2Mc values of Hermans et al. Such an uncertainty in the adduct stability translates into a factor of ten uncertainty in $K_1(220$ K). Hence, the values of K_1 reported by Hermans et al. lie at the upper-end of a large (\sim order of magnitude) spread of calculated values, and may therefore represent upper-limits. Consequently we have used Hermans et al. parameters to assess the likely maximum impact of HO₂-mediated CH₃C(O)CH₃ depletion on the chemistry of the atmosphere (see Sect. 3.3). The impact of the uncertainty on the theoretically derived rearrangement Reaction (R1b) is less significant; while the new theoretical data suggests a somewhat higher barrier with consequently slower adduct formation, this would not affect the impact of (R1) on the atmosphere. For experimental studies, a slower k_{1b} does increase interference of bimolecular reactions of the complex.

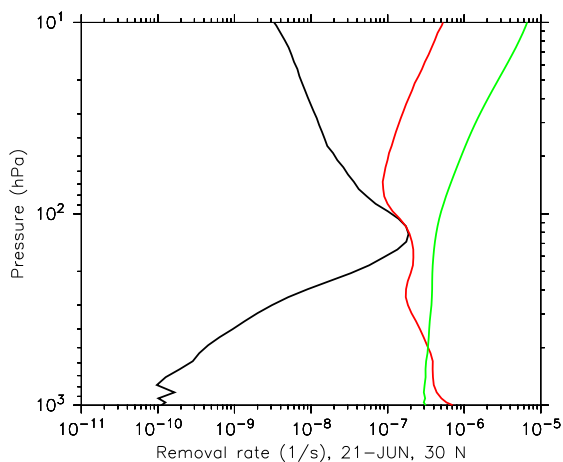
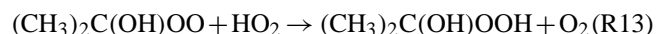


Fig. 5. CH₃C(O)CH₃ removal rates at 30° N solstice initiated by: photolysis (R3) in green; reaction with OH (R4) in red; and in black the reaction of interest (R1) using k_1 and K_1 parameters from (Hermans et al., 2004). See Sect. 3.3 for details.

3.3 Modelling studies

The modelling focused on the role of (R1) as an CH₃C(O)CH₃ degradation process in the UT and its potential as a source of CH₃C(O)OH, as postulated by Hermans et al. (2004). The simulation S0, which has been extensively described and evaluated previously (Jöckel et al., 2006; Pozzer et al., 2007) was used as a point of reference. A further two simulations were performed using augmented chemical mechanisms. In simulation SR1, the chemical mechanism (Sander et al., 2005) was updated to account for recent developments in peroxy radical chemistry (see Table 1 for details). In simulation SR2 the chemical mechanism was extended to include the reactions of interest from this work: (R1), (R2) and the reaction (R13) of HO₂ with (CH₃)₂C(OH)OO, a minor additional pathway for trapping peroxy radicals formed in (R1).



Note that the HO₂-CH₃C(O)CH₃ complex was not explicitly treated in this work, as its reactions, e.g. the proposed (R12) do not degrade CH₃C(O)CH₃. As was discussed in Sect. 3.2 above, large uncertainties remain in the magnitude of $K_1(T)$, the crucial parameter for determining atmospheric impact. In this work the largest published values of K_1 (Hermans et al. 2004) were used in order to assess the likely maximum impact of (R1) on the chemistry of the troposphere.

Figure 5 displays the calculated removal rate for CH₃C(O)CH₃ at 30° North on 21 June 2000, based on the results of the SR2 simulation. The largest removal rates due to (R1) are located in the UT (where the lowest temperature conditions are found), with a maximum at around 100 hPa where a similar rate to that of photolysis (R3) and reaction with OH (R4) was calculated. This compares well with the

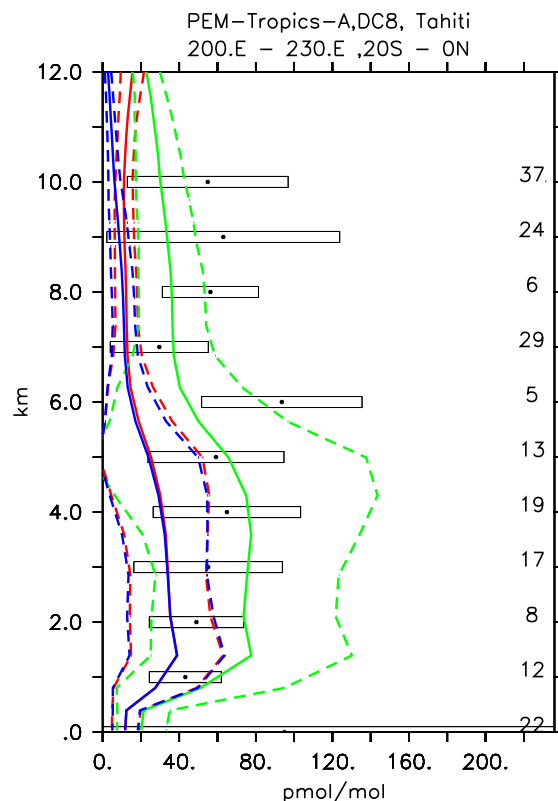


Fig. 6. Vertical profiles of CH₃C(O)OH (nmol mol⁻¹) from simulations and observations. Asterisks and boxes represent the average and the standard deviation (with respect to space and time) of the measurements from a specific region (Tahiti) taken during the PEM Tropics-A campaign. On the right side the number of measurements for the specific region is listed. The simulated average is indicated by the line and the corresponding standard deviation with respect to time and space by the dashed lines. The blue, red and green lines represent model results from simulations SR1, SR2 and S0, respectively.

previous modelling study by Hermans et al. (2005) who calculated 30 % of CH₃C(O)CH₃ degradation was due to (R1) at the tropopause. As was noted in Sect. 1 however, the yield of HO_x from (R1–R2) is considerably smaller than that from either photolysis (R3) or OH + CH₃C(O)CH₃ (R4); we therefore conclude that (R1) may make only a small contribution to radical production in the UT.

The contribution of (R1) to CH₃C(O)OH formation, was similarly found to be greatest in the coolest regions. Updating the chemical mechanism with new kinetic data resulted in reduced production rates and enhanced loss rates of CH₃C(O)OH, thus dramatically decreasing its mixing ratio and increasing the discrepancies between observation and simulation. This is illustrated in Fig. 6 where we show a comparison of simulated values obtained using S0, SR1 and SR2 from this work, with observations, taken from the PEM-Tropics-A campaign (Hoell et al., 1999). While simulation

SO is in reasonable agreement with the observations, updating the chemical mechanism (SR1) leads to a substantially smaller CH₃C(O)OH mixing ratio throughout the troposphere. Figure 6 also displays the smaller (in absolute terms) but still significant change in modelled CH₃C(O)OH upon inclusion of (R1) chemistry (the red line, SR2). The effects are insignificant at low altitudes, and CH₃C(O)OH observations (e.g. at 6 and 8 km) are not reproduced despite the generous uncertainties quoted for both model and measurement output. Note however that above 10 km more than 50 % of modelled CH₃C(O)OH mixing ratio may be attributed to reaction of CH₃C(O)CH₃ with HO₂.

The simulated rates of formation of CH₃C(O)OH will depend critically on the model levels of NO_x and organic precursors for the acetylperoxy (CH₃C(O)O₂) radical. Thus, the model output for NO, the levels of which determine whether CH₃C(O)O₂ reacts with NO or with HO₂ to form CH₃C(O)OH, were compared with measurements in the same region. Likewise, PAN, formed from combination of CH₃C(O)O₂ with NO₂ may be considered an indicator of rates of CH₃C(O)O₂ formation and a comparison between observation and model was also conducted. In both cases, the model was able to reproduce the observed levels of NO and PAN reasonably well, suggesting no important omissions in the model code in this regard. Exemplary plots are provided in the Supplement to illustrate this. Given that the kinetic database on CH₃C(O)OH removal by OH is now in good shape, the model-observation discrepancy is most likely due to missing source terms. Recent model calculations by Paulot et al. (2011) also underestimated CH₃C(O)OH compared to observations. The authors postulated that organic aerosols could balance the CH₃C(O)OH budget, accounting for as much as 50 % of total CH₃C(O)OH emissions. This hypothesis is backed-up by the ubiquitous model underestimation of CH₃C(O)OH throughout the atmosphere which is indicative of a slow secondary CH₃C(O)OH formation, rather than a source concentrated in the upper troposphere as postulated by Hermans et al. Further clarification of the atmospheric chemistry of CH₃C(O)OH, whilst beyond the scope of this study, is clearly necessary.

4 Conclusions

The reaction HO₂ + CH₃C(O)CH₃ (CH₃)₂C(OH)OO (R1) was, for the first time, experimentally investigated in low-temperature conditions representative of the upper-troposphere. Evidence of reaction was observed only in the lowest temperature experiments, allowing a lower limiting value of $k_1(207\text{ K}) \approx 2 \times 10^{-12} \text{ cm}^3 \text{ molecule}^{-1} \text{ s}^{-1}$ to be estimated, in line with the theoretical predictions of Hermans et al. (2004). At temperatures above 230 K there was no observable interaction. Simulations were conducted which suggest these observations were consistent with HO₂-CH₃C(O)CH₃ complex formation (R1a), meaning that experimental evi-

dence for the crucial second step of rearrangement to peroxy radical (R1b) is still lacking. Results from new theoretical work demonstrate the large uncertainties inherent in calculating K_1 at $T < 220\text{ K}$. Atmospheric modelling studies using the largest reported K_1 values demonstrated that whilst (R1) may play a role in CH₃C(O)CH₃ removal and consequent CH₃C(O)OH formation at the tropopause, it does not explain observations of CH₃C(O)OH throughout the troposphere.

Supplementary material related to this article is available online at:
<http://www.atmos-chem-phys.net/12/1339/2012/acp-12-1339-2012-supplement.zip>.

Acknowledgements. We would like to thank all contributors to the ACPD online discussion for their helpful and insightful comments. In particular we thank J. Peeters for his insight into (R1) chemistry, and considerable advice and assistance in the preparation of the manuscript. This work was initiated as part of the EU integrated project SCOUT-O₃. A. P. thanks the International Max-Planck Research School for support. L. V. thanks the Max Planck Graduate Center for financial support.

The service charges for this open access publication have been covered by the Max Planck Society.

Edited by: N. M. Donahue

References

- Aloisio, S. and Francisco, J. S.: Complexes of Hydroxyl and Hydroperoxyl Radical with Formaldehyde, Acetaldehyde, and Acetone, *J. Phys. Chem. A*, 104, 3211–3224, 2000.
- Arnold, F., Knop, G., and Ziereis, H.: Acetone measurements in the upper troposphere and lower stratosphere – implications for hydroxyl radical abundances, *Nature*, 321, 505–507, 1986.
- Arnold, S. R., Chipperfield, M. P., and Blitz, M. A.: A three-dimensional model study of the effect of new temperature-dependent quantum yields for acetone photolysis, *J. Geophys. Res.-Atmos.*, 110, D22305 doi:10.1029/2005JD005998, 2005.
- Atkinson, R. and Arey, J.: Atmospheric degradation of volatile organic compounds, *Chem. Rev.*, 103, 4605–4638, 2003.
- Atkinson, R., Baulch, D. L., Cox, R. A., Crowley, J. N., Hampson, R. F., Hynes, R. G., Jenkin, M. E., Rossi, M. J., and Troe, J.: Evaluated kinetic and photochemical data for atmospheric chemistry: Volume I – gas phase reactions of O_x, HO_x, NO_x and SO_x species, *Atmos. Chem. Phys.*, 4, 1461–1738, doi:10.5194/acp-4-1461-2004, 2004.
- Atkinson, R., Baulch, D. L., Cox, R. A., Crowley, J. N., Hampson, R. F., Hynes, R. G., Jenkin, M. E., Rossi, M. J., Troe, J., and IUPAC Subcommittee: Evaluated kinetic and photochemical data for atmospheric chemistry: Volume II - gas phase reactions of organic species, *Atmos. Chem. Phys.*, 6, 3625–4055, doi:10.5194/acp-6-3625-2006, 2006.
- Benson, S. W.: Some observations on the kinetics and thermochemistry of the reactions of HO₂ radicals with aldehydes and ketones, *Int. J. Chem. Kinet.*, 33, 509–512, 2001.

- Blitz, M. A., Heard, D. E., Pilling, M. J., Arnold, S. R., and Chipperfield, M. P.: Pressure and temperature-dependent quantum yields for the photodissociation of acetone between 279 and 327.5 nm, *Geophys. Res. Lett.*, 31, L06111, doi:10.1029/2003GL018793, 2004
- Carr, S. A., Glowacki, D. R., Liang, C., Baeza-Romero, M. T., Blitz, M. A., Michael, J., Pilling, M. J., and Seakins, P. W.: Experimental and Modeling Studies of the Pressure and Temperature Dependences of the Kinetics and the OH Yields in the Acetyl + O₂ Reaction, *J. Phys. Chem. A*, 115, 1069–1085, 2011.
- Christensen, L. E., Okumura, M., Hansen, J. C., Sander, S. P., and Francisco, J. S.: Experimental and ab Initio Study of the HO₂·CH₃OH Complex: Thermodynamics and Kinetics of Formation, *J. Phys. Chem. A* 110, 6948–6959, 2006.
- Cours, T., Canneaux, S., and Bohr, F.: Features of the potential energy surface for the reaction of HO₂ radical with acetone, *Int. J. Quantum Chem.*, 107, 1344–1354, 2007.
- Curtis, A. R. and Sweetenham, W. P.: Facsimile, AERE, Report (R-12)805, 1987.
- Dillon, T. J. and Crowley, J. N.: Direct detection of OH formation in the reactions of HO₂ with CH₃C(O)O₂ and other substituted peroxy radicals, *Atmos. Chem. Phys.*, 8, 4877–4889, doi:10.5194/acp-8-4877-2008, 2008.
- Dillon, T. J., Hölscher, D., Sivakumaran, V., Horowitz, A., and Crowley, J. N.: Kinetics of the reactions of HO with methanol (210–351 K) and with ethanol (216–368 K), *Phys. Chem. Chem. Phys.*, 7, 349–355, 2005.
- Dillon, T. J., Horowitz, A., Hölscher, D., and Crowley, J. N.: Reaction of HO with hydroxyacetone (HOCH₂C(O)CH₃): rate coefficients and mechanism, *Phys. Chem. Chem. Phys.*, 8, 236–246, 2006.
- Fry, J. L., Nizkorodov, S. A., Okumura, M., Roehl, C. M., Francisco, J. S., and Wennberg, P. O.: Cis-cis and trans-perp HOONO: Action spectroscopy and isomerization kinetics, *J. Chem. Phys.*, 121, 1432–1448, 2004.
- Grieman, F. J., Noell, A. C., Davis-Van Atta, C., Okumura, M., and Sander, S. P.: Determination of Equilibrium Constants for the Reaction between Acetone and HO₂ Using Infrared Kinetic Spectroscopy, *J. Phys. Chem. A*, 115, 10527–10538, 2011.
- Gierczak, T. and Ravishankara, A. R.: Does the HO₂ radical react with ketones?, *Int. J. Chem. Kinet.*, 32, 573–580, 2000.
- Gierczak, T., Burkholder, J. B., Bauerle, S., and Ravishankara, A. R.: Photochemistry of acetone under tropospheric conditions, *Chem. Phys.*, 231, 229–244, 1998.
- Gierczak, T., Gilles, M. K., Bauerle, S., and Ravishankara, A. R.: Reaction of hydroxyl radical with acetone. 1. Kinetics of the reactions of OH, OD, and (OH)-O-18 with acetone and acetone-D(6), *J. Phys. Chem. A*, 107, 5014–5020, 2003.
- Hasson, A. S., Tyndall, G. S., and Orlando, J. J.: A product yield study of the reaction of HO₂ radicals with ethyl peroxy (C₂H₅O₂), acetyl peroxy (CH₃C(O)O₂), and acetonyl peroxy (CH₃C(O)CH₂O₂) radicals, *J. Phys. Chem. A*, 108, 5979–5989, 2004.
- Hermans, I., Nguyen, T. L., Jacobs, P. A., and Peeters, J.: Tropopause chemistry revisited: HO₂-initiated oxidation as an efficient acetone sink, *J. Am. Chem. Soc.*, 126, 9908–9909, 2004.
- Hermans, I., Muller, J. F., Nguyen, T. L., Jacobs, P. A., and Peeters, J.: Kinetics of alpha-hydroxy-alkylperoxyl radicals in oxidation processes. HO₂-initiated oxidation of ketones/aldehydes near the tropopause, *J. Phys. Chem. A*, 109, 4303–4311, 2005.
- Hoell, J. M., Davis, D. D., Jacob, D. J., Rodgers, M. O., Newell, R. E., Fuelberg, H. E., McNeal, R. J., Raper, J. L., and Bendura, R. J.: Pacific Exploratory Mission in the tropical Pacific: PEM-Tropics A, August–September 1996, *J. Geophys. Res.-Atmos.*, 104, 5567–5583, 1999.
- IUPAC Subcommittee for gas kinetic data evaluation (Ammann, M., Atkinson, R., Cox, R. A., Crowley, J. N., Hynes, R. G., Jenkin, M. E., Mellouki, W., Rossi, M. J., Troe, J., and Wallington, T. J.): Evaluated kinetic data: <http://www.iupac-kinetic.ch.cam.ac.uk/>, 2011.
- Jacob, D. J., Field, B. D., Jin, E. M., Bey, I., Li, Q., Logan, J. A., Yantosca, R. M., and Singh, H. B.: Atmospheric budget of acetone, *J. Geophys. Res.*, 107, 4100, doi:10.1029/2001JD000694, 2002.
- Jenkin, M. E., Hurley, M. D., and Wallington, T. J.: Investigation of the radical product channel of the CH₃C(O)CH₂O₂+HO₂ reaction in the gas phase, *Phys. Chem. Chem. Phys.*, 10, 4274–4280, 2008.
- Jeuken, A., Siegmund, P., Heijboer, L., Feichter, J., and Bengtsson, L.: On the potential assimilating meteorological analyses in a global model for the purpose of model validation, *J. Geophys. Res.*, 101, 16939–16950, 1996
- Jöckel, P., Sander, R., Kerkweg, A., Tost, H., and Lelieveld, J.: Technical Note: The Modular Earth Submodel System (MESSy) – a new approach towards Earth System Modeling, *Atmos. Chem. Phys.*, 5, 433–444, doi:10.5194/acp-5-433-2005, 2005.
- Jöckel, P., Tost, H., Pozzer, A., Brühl, C., Buchholz, J., Ganzeveld, L., Hoor, P., Kerkweg, A., Lawrence, M. G., Sander, R., Steil, B., Stiller, G., Tanarhte, M., Taraborrelli, D., van Aardenne, J., and Lelieveld, J.: The atmospheric chemistry general circulation model ECHAM5/MESSy1: consistent simulation of ozone from the surface to the mesosphere, *Atmos. Chem. Phys.*, 6, 5067–5104, doi:10.5194/acp-6-5067-2006, 2006.
- Lelieveld, J., Brühl, C., Jöckel, P., Steil, B., Crutzen, P. J., Fischer, H., Giorgetta, M. A., Hoor, P., Lawrence, M. G., Sausen, R., and Tost, H.: Stratospheric dryness: model simulations and satellite observations, *Atmos. Chem. Phys.*, 7, 1313–1332, doi:10.5194/acp-7-1313-2007, 2007.
- Maricq, M. M. and Szente, J. J.: The UV spectrum of acetyl and the kinetics of the chain reaction between acetaldehyde and chlorine, *Chem. Phys. Lett.*, 253, 333–339, 1996.
- McKeen, S. A., Gierczak, T., Burkholder, J. B., Wennberg, P. O., Hanisco, T. F., Keim, E. R., Gao, R.-S., Liu, S. C., Ravishankara, A. R., and Fahey, D. W.: The photochemistry of acetone in the upper troposphere: A source of odd-hydrogen radicals, *Geophys. Res. Lett.*, 24, 3177–3180, 1997.
- Nesbitt, F. L., Payne, W. A., and Stief, L. J.: Temperature-Dependence for the Absolute Rate-Constant for the Reaction CH₂OH+O₂ → HO₂+H₂CO from 215 K to 300 K, *J. Phys. Chem.*, 92, 4030–4032, 1988.
- Orlando, J. J., Tyndall, G. S., Vereecken, L., and Peeters, J.: The Atmospheric Chemistry of the Acetonyl Radical, *J. Phys. Chem. A*, 104, 11578–11588, 2000.
- Paulot, F., Wunch, D., Crouse, J. D., Toon, G. C., Millet, D. B., DeCarlo, P. F., Vigouroux, C., Deutscher, N. M., González Abad, G., Notholt, J., Warneke, T., Hannigan, J. W., Warneke, C., de Gouw, J. A., Dunlea, E. J., De Mazière, M., Griffith, D. W. T., Bernath, P., Jimenez, J. L., and Wennberg, P. O.: Im-

- portance of secondary sources in the atmospheric budgets of formic and acetic acids, *Atmos. Chem. Phys.*, 11, 1989–2013, doi:10.5194/acp-11-1989-2011, 2011.
- Pozzer, A., Jöckel, P., Tost, H., Sander, R., Ganzeveld, L., Kerkweg, A., and Lelieveld, J.: Simulating organic species with the global atmospheric chemistry general circulation model ECHAM5/MESSy1: a comparison of model results with observations, *Atmos. Chem. Phys.*, 7, 2527–2550, doi:10.5194/acp-7-2527-2007, 2007.
- Sander, R., Kerkweg, A., Jöckel, P., and Lelieveld, J.: Technical note: The new comprehensive atmospheric chemistry module MECCA, *Atmos. Chem. Phys.*, 5, 445–450, doi:10.5194/acp-5-445-2005, 2005.
- Singh, H. B., Kanakidou, M., Crutzen, P. J., and Jacob, D. J.: High concentrations and photochemical fate of oxygenated hydrocarbons in the global troposphere, *Nature*, 378, 50–54, 1995.
- Talukdar, R. K., Gierczak, T., McCabe, D. C., and Ravishankara, A. R.: Reaction of Hydroxyl Radical with Acetone. 2. Products and Reaction Mechanism, *J. Phys. Chem. A*, 107, 5021–5032, 2003.
- Timonen, R.: Kinetics of the reactions of some polyatomic free radicals with Cl₂ and Br₂, and reactions of formyl radicals with O₂, NO₂, Cl₂, Br₂, and H atoms, *Ann. Acad. Sci. Fenn. Ser. A2*, 218, 5–45, 1988.
- Tomas, A., Villenave, E., and Lesclaux, R.: Reactions of the HO₂ radical with CH₃CHO and CH₃C(O)O₂ in the gas phase, *J. Phys. Chem. A*, 105, 3505–3514, 2001.
- Veyret, B., Lesclaux, R., Rayez, M.-T., Rayez, J.-C., Cox, R. A., and Moortgat, G. K.: Kinetics and mechanism of the photooxidation of formaldehyde. 1. Flash photolysis study, *J. Phys. Chem.*, 93, 2368–2374, 1989.
- Wennberg, P. O., Hanisco, T. F., Jaeglé, L., Jacob, D. J., Hintsala, E. J., Lanzendorf, E. J., Anderson, J. G., Gao, R.-S., Keim, E. R., Donnelly, S. G., Del Negro, L. A., Fahey, D. W., McKeen, S. A., Salawitch, R. J., Webster, C. R., May, R. D., Herman, R. L., Profitt, M. H., Margitan, J. J., Atlas, E. L., Schauffler, S. M., Flocke, F., McElroy, C. T., and Bui, T. P.: Hydrogen radicals, nitrogen radicals, and the production of O₃ in the upper troposphere, *Science*, 279, 49–53, 1998.
- Wollenhaupt, M., Carl, S. A., Horowitz, A., and Crowley, J. N.: Rate coefficients for reaction of OH with acetone between 202 and 395 K, *J. Phys. Chem.*, 104, 2695–2705, 2000.